Surface Enhanced Raman Scattering on a Single Nanometric Aperture

ARTICLE *in* THE JOURNAL OF PHYSICAL CHEMISTRY C · OCTOBER 2010

Impact Factor: 4.77 · DOI: 10.1021/jp104971p · Source: OAI

Surface Enhanced Raman Scattering on a Single Nanometric Aperture

Nadia Djaker,[†] Richard Hostein,[†] Eloïse Devaux,[‡] Thomas W. Ebbesen,[‡] Hervé Rigneault,[†] and Jérôme Wenger*[,†]

Institut Fresnel, Aix-Marseille Université, CNRS, Ecole Centrale Marseille, Campus de St Jérome, 13397 Marseille, France, and Institut de Science et d'Ingénierie Supramoléculaires, Université de Strasbourg, CNRS, 8 allée G. Monge, 67000 Strasbourg, France

Received: May 31, 2010; Revised Manuscript Received: July 23, 2010

Arrays of nanoapertures have been demonstrated to realize efficient, robust, and reproducible substrates for surface-enhanced Raman scattering SERS spectroscopy. However, little attention has been devoted to single nanoapertures, although a thorough understanding of the SERS phenomenon in a single aperture is essential for the rationale optimization of nanoaperture arrays SERS. In this study, single nanoapertures milled in optically thick gold films are quantitatively evaluated for the first time to determine the SERS enhancement factors using para-mercaptoaniline as nonresonant analyte. We determine a peak enhancement factor of 2×10^5 for a single 100 nm diameter aperture. Although this is a moderate enhancement factor, we believe that nanoapertures deserve special attention to highlight the physical and chemical phenomena leading to SERS enhancement and better understand the design of nanoaperture arrays for SERS substrates. The experimental data are supported by numerical simulations and argue for a careful consideration of aperture diameter, incident polarization, analyte deposition method, and nature of the gold adhesion layer while designing aperture-based SERS substrates and evaluating SERS enhancement factors.

Introduction

Metallic nanostructures have attracted much interest over the last years to realize efficient and reproducible media for surface-enhanced Raman scattering (SERS) spectroscopy.[1] The major aim is to develop SERS substrates combining high sensitivity with control and localization of the regions leading to high SERS enhancement. A wide range of geometries are currently investigated, from nanoparticle arrays,[2−4] core−shell nanoparticles,[5,6] nanoaperture arrays,[7] bowtie antennas,[8] nanogaps,[9] and nanorings.[10] Among these different structures, nanoapertures milled in noble metal films realize promising substrates thanks to their rational and tunable design, controlled surface enhancement, surfactant-free fabrication, and intrinsic robustness. Over the last four years, a large number of studies have considered the implementation of nanoapertures arrays as SERS substrates.[7,11−19] However, there has been little consideration of the SERS enhancement brought by a single aperture.

Two previous studies consider isolated nanostructures for SERS that partly involve single apertures: the first focuses on combined aperture−nanoparticle pairs[20] and the second on double-hole structures.[21] In both cases, SERS enhancement factors up to 10^8 were reported. Although a single circular nanoaperture is not expected to yield such high factors, we still believe that it deserves special attention to highlight the phenomena leading to SERS enhancement and better understand the design of nanoaperture arrays for SERS substrates.

Here, we provide the first quantitative discussion on the SERS enhancement factors on single nanoapertures milled in optically thick gold films, and compare our results to numerical simulations. We use *para*-mercaptoaniline (pMA, also known as 4-aminothiophenol) as a Raman-active probe molecule because of its strong nonresonant Raman cross-section and because the thiol moiety is intended to form a self-assembled monolayer (SAM) upon binding to gold. The results discussed hereafter argue for a careful consideration of aperture diameter, incident polarization, molecular analyte deposition method, and nature of the gold adhesion layer while designing aperture-based SERS substrates and evaluating SERS enhancement factors.

Experimental Methods

Nanoapertures are milled by focused ion beam (FEI Strata DB235) on 200 nm thick gold films deposited using reactive DC magnetron sputtering on a cleaned 150 μm thick glass coverslip. Figure 1 displays a typical SEM view of the nanoaperture sample. For the data presented in this study, adhesion between the gold film and the glass substrate is ensured by a layer of 10 nm titanium dioxide TiO_2. Thickness control is maintained by a cluster of piezoelectric monitors, following a calibration of the deposition process using quartz crystal monitors and test samples.

To incubate the samples with pMA molecules and form SAM, we followed the procedure published by several groups.[6,8,9] pMA (4-Aminothiophenol, 97%, Aldrich) is used as received, diluted to 4 mM in HPLC grade ethanol (Sigma-Aldrich) and incubated for 12 h at room temperature on a freshly cleaned nanoaperture sample. Incubated samples are then rinsed with clean ethanol and dried with pure nitrogen. The chamber holding the sample is finally covered with argon to avoid pMA oxidation.

The home-built confocal Raman microspectrometer used in this study is based on an inverted microscope with 40× 1.3NA oil immersion objective (Zeiss Apochromat). The excitation source is provided by a continuous wave HeNe laser operating at 632.8 nm. For all of the experiments presented here, the laser power is set to 1 mW at the microscope entrance to avoid damaging the sample, and the laser polarization is controlled by a polarizer followed by half- and quarter-waveplates. The

* To whom correspondence should be addressed. E-mail: jerome.wenger@Fresnel.fr.
[†] Aix-Marseille University.
[‡] Strasbourg University.

10.1021/jp104971p
Published on Web 09/09/2010

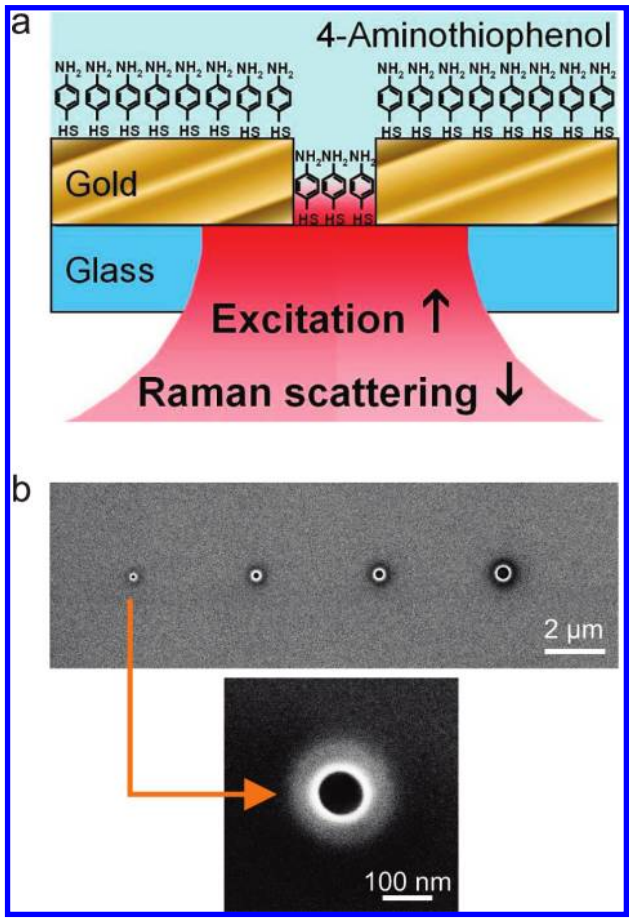

Figure 1. (a) Schematic description of the experimental configuration to probe a single aperture. (b) Scanning electron microscope of some aperture samples.

Raman scattered light is collected by the same microscope objective and is further separated from the excitation laser and elastically scattered light by a set formed by a dichroic mirror (Omega Filters 650DRLP), long-pass filter (Omega Filters 640AELP), and holographic notch filter (Kaiser Optical HNF-632.8−1.0). Overall, the attenuation of the laser line corresponds to an optical density greater than 9. A 50 μm pinhole conjugated to the microscope objective focal plane rejects the out-of-focus light, and defines a confocal volume calibrated to 0.75 fL. The Raman signal is then directed toward a Jobin-Yvon 270 M spectrometer (grating 600 grooves per mm) coupled with a liquid-nitrogen-cooled CCD camera (SpectrumOne, Jobin-Yvon). The spectrometer entrance slit is conjugated to the confocal pinhole with a 1:1 magnification. This configuration allows for all of the light passing through the confocal pinhole to enter the spectrometer with the optimum spectrometer resolution of 0.3 nm (or 7 cm^{-1} in our case). For each measurement, the integration time is set to 30 s.

Three-dimensional numerical modeling on nanoapertures is based on the finite-difference time-domain FDTD method using Rsoft Fullwave version 6.0. The model considers a computational space of $0.4 \times 0.4 \times 0.4$ μ m^3, perfect matched layers boundary conditions on all faces, 2 nm cell size, and a total computational time of 20 periods of light. Excitation at 632.8 nm is launched incoming from the bottom with a flat phase. Gold dielectric properties are incorporated as measured by spectroscopic ellipsometry.[33] Depending on the model being used (see Figure 4), the refractive index of the medium inside the nanoaperture is set to $n_{in} = 1.0$ ("SAM" model) or $n_{in} = 1.5$ ("bulk" model). Adequation to independent simulations based on finite elements ensure relevance of the results.[22]

Results and Discussion

Representative SERS spectra of pMA on single nanoapertures of decreasing diameters are shown in Figure 2. The two main Raman bands of pMA at 1090 and 1600 cm^{-1} are clearly seen above the background. Following previous pMA mode assignments,[23,24] the modes at 1090 and 1600 cm^{-1} are assigned to a_1 symmetry. These modes have been demonstrated to be less

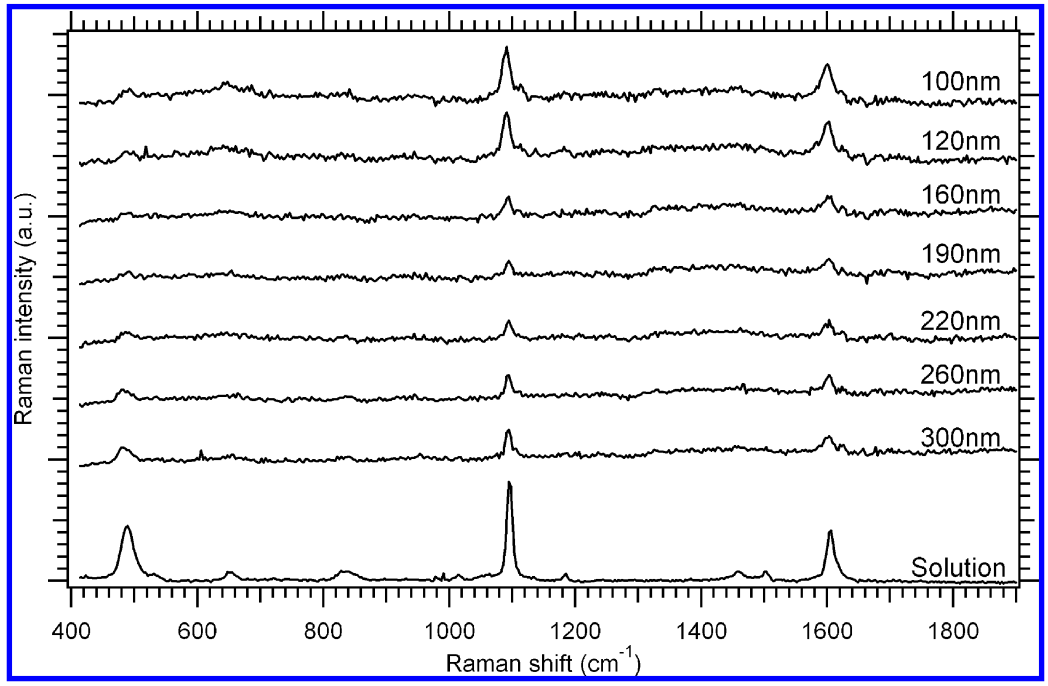

Figure 2. Typical SERS spectra of pMA on single gold nanoapertures of decreasing diameters, and reference Raman spectra in 1.5 M ethanol solution. The excitation wavelength is 632.8 nm, the cw laser power is 1 mW at the microscope entrance, and the integration time is 30 s. We use the intensity of the Raman band at 1090 cm^{-1} to compute the SERS enhancement factor.

influenced by charge transfer effects than modes at 1140, 1190, and 1450 cm^{-1} assigned to b_2 symmetry.[8,25] Hereafter, we thus use the Raman band at 1090 cm^{-1} to quantify the SERS enhancement factor. Each Raman spectrum is analyzed by subtracting the baseline from the peak intensity and dividing by the experiment acquisition time and average excitation power. We confirmed experimentally that the measured SERS intensity grows linearly with excitation power and data acquisition time. We point out that a variability in SERS intensity of less than 12% was measured from aperture to aperture, and results mostly from minor nanofabrication deficiencies.

A general expression to estimate the SERS enhancement factor EF amounts to compare the number of Raman scattered photons per second and per molecule[26,27]

$$\mathrm{EF} = \frac{I_{\mathrm{sers}}/N_{\mathrm{sers}}}{I_{\mathrm{ref}}/N_{\mathrm{ref}}} \quad (1)$$

where I_{sers} and I_{ref} are the normalized Raman intensities (integrated intensity over the whole Raman peak at 1090 cm^{-1} divided by the experiment integration time and the laser power) for the same Raman band on the SERS and reference experiments, that are unambiguously measured from the spectra as displayed in Figure 2. N_{sers} and N_{ref} are the number of molecules contributing to the detected signal in each case. N_{ref} is deduced from the concentration of the reference solution and the calibration of the confocal analysis volume. In our case, the reference solution concentration is 1.5 M and the confocal volume is 0.75 fL, which yields $N_{\mathrm{ref}} \simeq 6.8 \times 10^8$ molecules. Actually, the major difficulty in measuring EF amounts to estimate N_{sers}. Even for structures as conceptually simple as single circular apertures, various methods to compute N_{sers} can be considered, resulting in large differences in the estimated SERS enhancement factor. Apart from the specific case of single-molecule SERS, an essential difficulty in expressing a SERS enhancement factor over a given nanostructure is set by the highly heterogeneous electromagnetic intensity distribution, that induces large variations in the local SERS gain. The following discussion is closely linked to the in-depth study of SERS enhancement factors presented in.[27]

Estimating the SERS enhancement factor in a nanoaperture requires supplementary knowledge of the electromagnetic field distribution inside the nanoaperture to determine how many molecules contribute to the SERS signal. To this end, we have conducted several numerical simulations based on FDTD method as described in the Experimental Section. Figure 3 presents the electric field intensity $|E|^2$ distribution in the case of a 100 nm diameter aperture with excitation at 632.8 nm linearly polarized along x axis. As already observed in previous simulations,[13,19,28] the highest electric field is found to occur at the aperture edge, with two lobes oriented parallel to the excitation polarization corresponding to local charges accumulations. The maximum intensity enhancement obtained is around $|E_{\mathrm{max}}|^2/|E_0|^2 \sim 220$. The intensity is found to decay quasi-exponentially from the aperture rim with a characteristic attenuation distance of $d \sim 4$ nm, which appears similar to values already reported.[13,20] As we will discuss below, to experimentally determine the peak SERS enhancement, we restrict the electromagnetic intensity distribution inside the nanoaperture to the high intensity region close to the aperture rim. We use the following model for the field intensity distribution inside the aperture (in cylindrical coordinates):

$$I_{\mathrm{aper}}(r,\theta,z) = |E_{\mathrm{max}}|^2 e^{-(R-r)/d} \cos^2\theta e^{-z/d} \quad (2)$$

where R denotes the aperture radius, and d the decay length from the aperture rim. This expression states that the intensity is exponentially decaying from the aperture rim (we numerically found $d \sim 4$ nm in both radial and vertical directions, so for the cases studied here $R \gg d$). The $\cos^2\theta$ term originates from the linear polarization of the excitation field (this term is absent for a circular polarization). These spatial features can be seen on the simulations in Figure 3.

We first attempt to estimate experimentally the peak SERS enhancement factor close to the aperture rim, and compare it to the maximum enhancement factor deduced from the numerical simulations. To this end, we need to evaluate an effective number of molecules N_{sers} that corresponds to the number of molecules contributing to the signal if all of them were residing at the position of maximum enhancement. As the Raman intensity is approximately proportional to the square of the local excitation intensity, the expression of N_{sers} involves the square factor of the intensity distribution inside the aperture, as given by eq 2. To fully estimate N_{sers}, it is also necessary to consider the way the pMA molecules fill the structure. First, we assume that only the gold-air surface is covered by a single monolayer of pMA ("SAM" or surface model). This is what our preparation procedure is intended to realize. For this model, N_{sers} is expressed

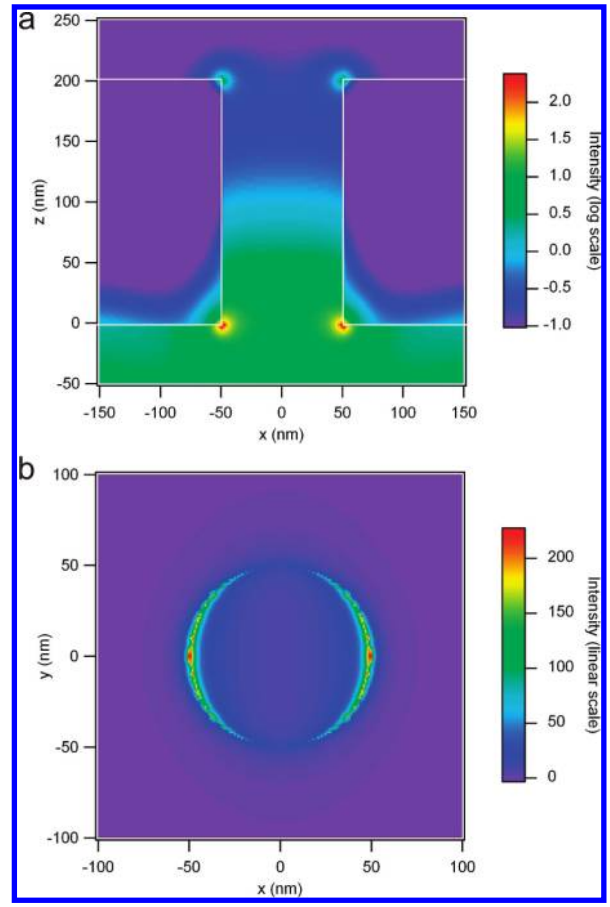

Figure 3. Three-dimensional finite-difference-time-domain numerical simulations of the electric field intensity distribution for a single 100 nm diameter aperture milled in 200 nm-thick gold film, immersed in a homogeneous medium of 1.5 refractive index. Excitation is performed from below, with linear polarization along the x direction. (a) Vertical cut along the incident polarization direction. (b) Horizontal cut at the gold film lower surface.

from the square of the field intensity distribution inside the aperture (eq 2):

$$N_{\text{sers,SAM}} = \frac{1}{\rho_S} R \int_0^{2\pi} \int_0^H [\cos^2\theta e^{-z/d}]^2 \, d\theta \, dz \approx \frac{1}{\rho_S} \frac{\pi R d}{2} \quad (3)$$

where ρ_S is the pMA surface density per molecule and H is the aperture height. ρ_S is taken from the literature to 0.19 nm^2/molecule.[6,8,23,24] Second, another approach considers that the bottom volume of the nanoaperture is filled by dense dense pMA molecules, at least over a region larger than the attenuation distance d (this is referred to as "bulk" or volume model). For this model, N_{sers} is expressed as

$$N_{\text{sers,bulk}} = \frac{1}{\rho_V} \int_0^R \int_0^{2\pi} \int_0^H [e^{-(R-r)/d} \cos^2\theta e^{-z/d}]^2 r \, dr \, d\theta \, dz \approx \frac{1}{\rho_V} \frac{\pi R d^2}{4} \quad (4)$$

where ρ_V is the pMA volume density per molecule. $\rho_V = 0.2$ nm^3/molecule is deduced from the pMA density (1.06 g/cm^3) and molecular mass (125 g/mol). These two models for N_{sers} result in estimates that differ by about a factor of 2, inducing a difference in the estimated enhancement factor by the same amount. Typically, for a 100 nm diameter aperture, the effective numbers of SERS-active molecules are estimated to $N_{\text{sers, SAM}} \simeq 1600$ and $N_{\text{sers, bulk}} \simeq 3100$ molecules. This difference may seem negligible regarding the high enhancement factors typically involved in SERS experiments, yet we will show hereafter that the two models involve a noticeable difference when comparing with the numerical simulations.

Figure 4 presents the experimental peak SERS enhancement factor EF_{peak} as function of the nanoaperture diameter for linear laser polarization and for the two "SAM" and "bulk" models. Since the "SAM" model considers a smaller number of contributing molecules N_{sers}, the enhancement factor is thus larger, and peaks at about 3.5×10^5 for a 100 nm aperture. This value can be considered as a maximum estimate for the experimental SERS enhancement factor on a 100 nm gold aperture. The experimental data in Figure 4, panels a and b, also demonstrate a growing dependence of EF_{peak} as the aperture diameter is reduced from 300 to 100 nm. This arguments for a careful consideration of the diameter while designing aperture-based SERS substrates. We stress that our approach considers that only the molecules located near the maximum points of electromagnetic field (aperture rim) contribute to the SERS signal. The aforementioned effective number of molecules N_{sers} correspond to the number of molecules contributing to the signal if all of them were residing at the position of maximum enhancement. This results from the peculiar shape of the field intensity distribution inside the aperture, as seen in Figure 3. These estimates for N_{sers} are thus only intended to be used to estimate the peak SERS enhancement factor.[27]

To compare the experimental results with the numerical simulations, Figure 4 also displays the peak enhancement factors derived from FDTD calculations for the two "SAM" and "bulk" models. The numerical estimates of EF_{peak} are obtained from $(|E_{\max}|/|E_0|)^4$ times a supplementary factor η_κ to taken to 2 for the range of aperture diameters investigated here. This factor

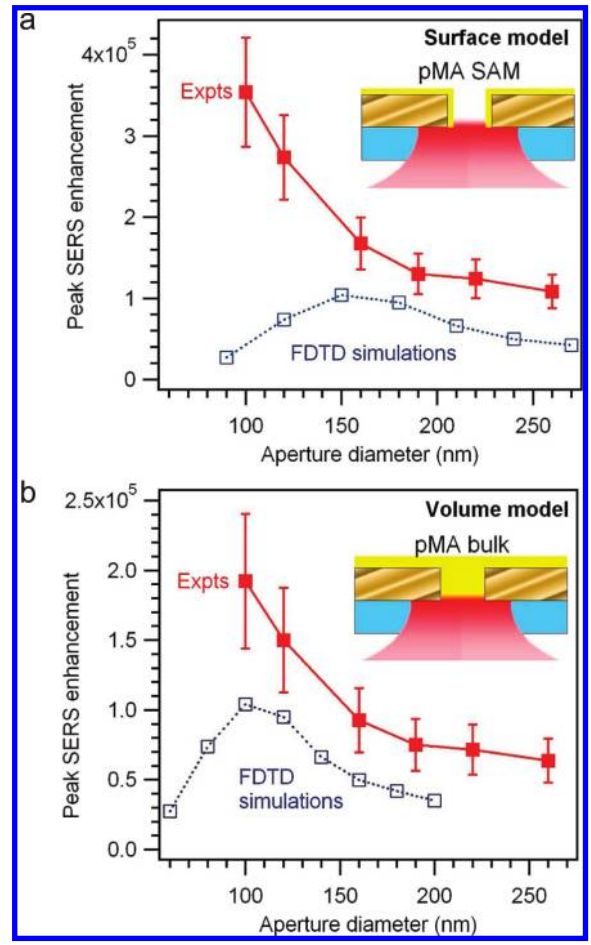

Figure 4. Peak SERS enhancement factor as function of nanoaperture diameter for linear laser polarization, deduced from the Raman intensity at 1090 cm^{-1}. Filled markers denote experimental data, empty squares are the enhancement factors deduced from FDTD simulations. (a) considers the model with pMA self-assembled on monolayers on the gold surface, whereas (b) assumes that all of the aperture volume is filled with pMA. In case (a) the refractive index of the medium inside the aperture is taken to $n_{\text{in}} = 1.0$, whereas in case (b) we assume $n_{\text{in}} = 1.5$. The error bars indicated here take into account the standard deviations of the measured Raman intensities I_{sers}, together with the influence of the uncertainties on R and d in the estimation of the SERS enhancement factor (the relative uncertainties on I_{sers}, R, and d amount to 12%, 5%, and 15%, respectively).

η_κ accounts for the gain in the collection efficiency brought by the nanoaperture which redirects more energy toward the detectors. The gain in collection efficiency is taken to agree with our previous studies on fluorescence in nanoapertures.[29,30] It is interesting to note that the numerical simulations predict an optimum diameter leading to the maximum field enhancement at the aperture edge. Similar to the case of fluorescence enhancement by nanoapertures,[29] the optimum aperture diameter depends on the excitation wavelength, the metal used, and the refractive index of the medium inside the aperture. We find that the optimum case (as indicated by the numerical simulations) corresponds to the diameter where the group velocity of the guided mode inside the aperture is close to zero, in close fashion to the results previously obtained for nanoaperture-enhanced fluorescence.[29] In the case of the "SAM" model, the refractive index of the medium inside the aperture is taken to $n_{\text{in}} = 1.0$, and consequently, the optimum diameter is predicted at 160 nm. In the case of the "bulk" model, we set $n_{\text{in}} = 1.5$, which gives

an optimum diameter at 110 nm. The two models thus differ noticeably for aperture diameters below 160 nm, as can be seen in Figure 4.

Comparing the numerical predictions with the experimental data, the "bulk" model displays a satisfactory correspondence with the experimental results (Figure 4b), whereas in the case of the "SAM" surface model (Figure 4a), there is a significant difference for the curve trend at aperture diameters below 160 nm. At least two explanations can be introduced to clarify this effect. First, the difference between the experimental and simulated EF could result from the contribution of a supplementary chemical enhancement factor, which is assumed to originate mostly from charge transfers to the metal, with values typically estimated around $10-10^2$. Second, one may question the realization of SAMs down to the bottom of the nanoapertures. Although we carefully applied the procedure described in refs 6, 8, and 9 and reproduced the results several times, the peculiar physical distribution of a nanoaperture with a height larger than its width may hinder the rinsing operation to remove the unbound molecules during the SAM-formation procedure. That would result in the lower volume within the nanoapertures being filled with unbound pMA molecules, while the top metal surface is being rinsed. Nanofluidic fluxes inside such nanodevices is still an open problem. We tend to preferentially select the "bulk" volume model because it matches the position of the aperture diameter where the SERS gain is expected to be maximum and displays a behavior consistent with our previous observations of nanoaperture-enhanced fluorescence.[29] To further confirm this "bulk" model, we have performed SERS experiments while the apertures are immersed in highly concentrated 100 M pMA solutions in ethanol, in order to mimic the situation in which the whole aperture is filled with molecules. The results show qualitatively the same behavior as the data in Figure 4b, with a growing enhancement factor up to 10^5 as the aperture diameter is reduced from 300 to 100 nm (data not shown). We never observed a dip for aperture diameters below 140 nm, as awaited from the "SAM" model. This discussion suggests that the formation of SAMs into complex structures such as nanoapertures is not trivial, and that care has to be taken to consistently check the presence of molecular SAMs.

Lastly, we would like to point out that if the laser polarization is switched to circular instead of linear, the total detected Raman intensity I_{sers} remains unchanged. However, the $\cos^2\theta$ terms in eqs 3 and 4 disappear, and the estimated numbers of molecules are $N_{sers,\,SAM,circ} \simeq \pi Rd/\rho_S$ and $N_{sers,bulk,circ} \simeq \pi Rd^2/2\rho_V$. These numbers are larger by approximately a factor of 2 as compared to the ones for linear polarization, meaning that a radially uniform illumination of the structure results in a larger number of scattering molecules. As a consequence, the peak enhancement factor for a circular laser polarization is half the enhancement factor for a linear polarization, given the same average laser excitation power. In the case of a linear laser polarization, all the driving power is focused into a region of minimum spatial extension, providing the maximum peak intensity $|E_{max}|^2$. For a circular polarization, the driving power is distributed over all the structure. The number of scattering molecules N_{sers} is twice larger, yet the peak intensity $|E_{max}|^2$ is two times smaller. The resulting detected total Raman intensity I_{sers} is the same as for linear polarization, but the peak enhancement factor is two times smaller. This further highlights the need for an accurate description of the model used to estimate N_{sers} and EF.

In the discussion above, we focus on the peak SERS enhancement factor for the molecules located close to the aperture rim. Another approach is to compute the average SERS enhancement factor over the whole aperture volume. As a conservative estimate, we consider that the aperture is filled with pMA molecules ("bulk" model discussed above). That way, the volume-averaged N_{sers} is expressed as

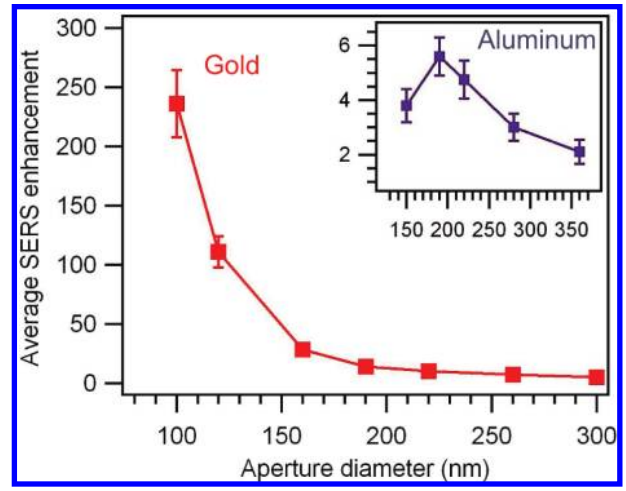

Figure 5. Average SERS enhancement factor as function of nanoaperture diameter, computed following eq 5, for apertures milled in gold. The inset compares with the results found for apertures milled in aluminum (excitation set to linear polarization).

$$N_{sers,avg} \simeq \frac{1}{\rho_V}\pi R^2 h \tag{5}$$

where h is the axial extension of the field intensity inside the aperture (typically h is computed to 60 nm for a 100 nm diameter aperture, up to 200 nm for a 200 nm diameter aperture). As a first approximation, the nanoaperture can be viewed as a cylindrical waveguide.[29] Therefore h corresponds to the characteristic attenuation length of the fundamental electromagnetic mode inside the nanoaperture waveguide. This quantity has not to be be confused this the decay length d from the aperture rim used earlier in the paper. Within this model the effects of laser polarization disappear, both linear and circular polarizations provide the same results. Figure 5 presents the volume-averaged enhancement factors deduced using this approach. As a consequence of the large number of molecules considered, the average enhancement factor is much lower than the peak EF and amounts to ~250 for an optimal diameter of 100 nm. These values can be compared (i) to the volume-averaged enhancement factors deduced from fluorescence characterization on gold nanoapertures and (ii) to the volume-averaged enhancement factor found for Raman scattering on nanoapertures milled in aluminum.

Single molecule fluorescence studies on nanoapertures have been used to determine the volume-averaged enhancement factors on the laser excitation intensity $(|E|/|E_0|)^2$, separately from the emission process.[30] A gain in local excitation intensity of about 3.5 is typically found for a single gold aperture.[31] The same procedure also provides an indication on the gain in collection efficiency of about 2 (the aperture acts as a nanoantenna, redirecting the emission toward the detectors). Altogether, these results can be used to infer an estimate of the volume-averaged SERS enhancement factor as $2 \times 3.5^2 \simeq 25$ deduced only from fluorescence-based experiments (this corresponds to the gain in collection efficiency times the gain in excitation intensity squared). It is apparent from Figure 5 that the volume-averaged Raman enhancement factor deduced from real SERS

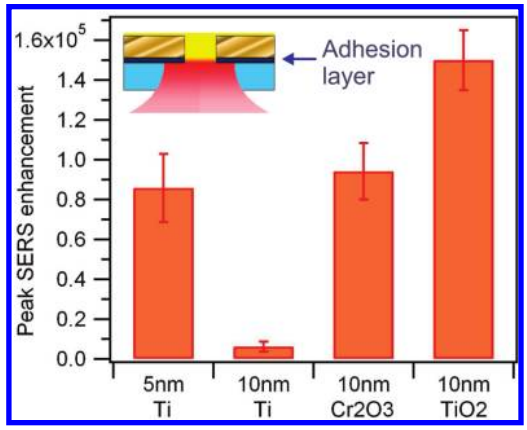

Figure 6. Influence of the nature of the adhesion layer used to ensure firm contact between the gold film and the underlying glass substrate. The data presents the peak enhancement factors obtained for a single 120 nm diameter aperture with linear excitation polarization, using the same model as in Figure 4b. The error bars indicated here only reflect the standard deviations of the measured Raman intensities I_{sers} from sample to sample, contrarily to Figure 4 where the error bars also consider the influence of the uncertainties on R and d in the estimation of the SERS enhancement factor.

measurements is higher by about 1 order of magnitude than the estimate obtained from fluorescence studies. This clearly stresses the difference between these two contrasts, and highlights the crucial contribution of the aperture rim in the case of SERS. To explain that latter affirmation, it must be kept in mind that the volume-averaged enhancement factor deduced from fluorescence measurements is only sensitive to the main electromagnetic mode inside the aperture and not to the high electromagnetic fields at the aperture rim (due to strong fluorescence quenching at the aperture rim). The discrepancy between the volume-averaged enhancement factors found for Raman scattering and fluorescence indicates that the mode inside the aperture is not the main source for the Raman emission, and that the aperture rim largely dominates the contribution to the SERS signal.

Second, the volume-averaged EF found for Raman scattering on gold can also be compared to the values previously obtained for Raman scattering on aluminum (see the insert in Figure 5).[32] Although a pure chlorobenzene solution was used instead of pMA in the case of aluminum apertures,[32] the large difference between the average EF in Figure 5 indicates that noble metals sustaining plasmonic resonances in the visible are obviously required to obtain strong SERS enhancement.

Lastly, we experimentally demonstrate a strong influence of the nature of the adhesion layer between the gold film and the glass substrate on the SERS enhancement factor. Thanks to their controlled shape, nanoapertures form a reliable structure to investigate the effects of the adhesion layer. We focus here on 120 nm diameter apertures with different adhesion layers between the gold film and the glass coverslip: 5 and 10 nm of titanium and 10 nm of chromium oxide (Cr_2O_3) and titanium oxide (TiO_2). We decide to compute here the peak SERS enhancement factor using the same model as in Figure 4b. Although the same preparation procedures and experimental setup are used, Figure 6 shows that the material permittivity and the thickness of the adhesion layer have a dramatic impact on the SERS enhancement factor. A difference greater than 30× is observed between the two extreme cases of 10 nm titanium and titanium oxide. Any increase in the electromagnetic absorption due to the adhesion layer material's properties or increased thickness lowers the SERS gains. We relate this effect to a damping of the energy coupling at the nanoaperture edge. Similar effects were numerically predicted in ref 33 and experimentally observed for nanoaperture-enhanced fluorescence.[31] This study further extends these results to the case of SERS spectroscopy, where the adhesion layer is shown to have an even more crucial effect. Most experimental studies of controlled SERS substrates skip the issue of the adhesion layer choice and design. Our observation however claim for a careful consideration of the adhesion layer while designing high-sensitivity SERS substrates.

Conclusions

A single circular nanoaperture is obviously not intended to provide ultrahigh SERS enhancement factors above 10^7 due to the lack of metal regions with high curvatures leading to strong charges accumulations, nevertheless it deserves special attention to highlight the phenomena leading to SERS enhancement and better understand the design of nanoaperture arrays for SERS substrates. In this contribution, we provide for the first time a quantitative evaluation of the SERS enhancement factors on single nanoapertures milled in optically thick gold films, and compare our results to numerical simulations. For a single 100 nm diameter aperture, we determine a peak SERS enhancement factor of 2×10^5. Altogether, our results argument for a careful considerations of aperture diameter, incident polarization, molecular analyte deposition method, and nature of the gold adhesion layer while designing aperture-based SERS substrates and evaluating SERS enhancement factors.

Acknowledgment. The authors acknowledge stimulating discussions with H. Aouani, S. Blair, N. Bonod, D. Gérard, and E. Popov. This research has been conducted in the scope of the CNRS-Weizmann NaBi European associated laboratory. It was partly funded by the French Agence Nationale de la Recherche under contract ANR-07-NANO-006-03 "ANTARES", and by the European Research Council under Contract 227577 "Plasmonics".

References and Notes

(1) Ko, H.; Singamaneni, S.; Tsukruk, V. V. Nanostructured Surfaces and Assemblies as SERS Media. *Small* **2008**, *4*, 1576–1599.

(2) Félidj, N.; Aubard, J.; Lévi, G.; Krenn, J. R.; Hohenau, A.; Schider, G.; Leitner, A.; Aussenegg, F. R. Optimized surface-enhanced Raman scattering on gold nanoparticle arrays. *Appl. Phys. Lett.* **2003**, *82*, 3095–3097.

(3) Yan, B.; Thubagere, A.; Premasiri, W. R.; Ziegler, L. D.; Dal Negro, L.; Reinhard, B. M. Engineered SERS Substrates with Multiscale Signal Enhancement: Nanoparticle Cluster Arrays. *ACS Nano* **2009**, *3*, 1190–1202.

(4) Gopinath, A.; Boriskina, S. V.; Reinhard, B. M.; Dal Negro, L. Deterministic aperiodic arrays of metal nanoparticles for surface-enhanced Raman scattering (SERS). *Opt. Express* **2009**, *17*, 3741–3753.

(5) Jackson, J. B.; Westcott, S. L.; Hirsch, L. R.; West, J. L.; Halas, N. J. Controlling the surface enhanced Raman effect via the nanoshell geometry. *Appl. Phys. Lett.* **2003**, *82*, 257–259.

(6) Jackson, J. B.; Halas, N. J. Surface-enhanced Raman scattering on tunable plasmonic nanoparticle substrates. *Proc. Natl. Acad. Sci. U.S.A.* **2004**, *101*, 17930–17935.

(7) Brolo, A. G.; Arctander, E.; Gordon, R.; Leathem, B.; Kavanagh, K. L. Nanohole-Enhanced Raman Scattering. *Nano Lett.* **2004**, *4*, 2015–2018.

(8) Fromm, D. P.; Sundaramurthy, A.; Kinkhabwala, A.; Schuck, P. J.; Kino, G. S.; Moerner, W. E. Exploring the chemical enhancement for surface-enhanced Raman scattering with Au bowtie nanoantennas. *J. Chem. Phys.* **2006**, *124*, 061101.

(9) Ward, D. R.; Grady, N. K.; Levin, C. S.; Halas, N. J.; Wu, Y.; Nordlander, P.; Natelson, D. Electromigrated Nanoscale Gaps for Surface-Enhanced Raman Spectroscopy. *Nano Lett.* **2007**, *7*, 1396–1400.

(10) Banaee, M. G.; Crozier, K. B. Gold nanorings as substrates for surface-enhanced Raman scattering. *Opt. Lett.* **2010**, *35*, 760–762.

(11) Reilly, T. H.; Rowlen, K. L. Investigation of nanoaperture arrays for use as SERS substrates. *Proc. SPIE* **2004**, *5513*, 250–257.

(12) Bahns, J. T.; Yan, F.; Qiu, D.; Wang, R.; Chen, L. Hole-Enhanced Raman Scattering. *Appl. Spectrosc.* **2006**, *60*, 989–993.

(13) Reilly, T. H.; Chang, S.-H.; Corbman, J. D.; Schatz, G. C.; Rowlen, K. L. Quantitative Evaluation of Plasmon Enhanced Raman Scattering from Nanoaperture Arrays. *J. Phys. Chem. C* **2007**, *111*, 1689–1694.

(14) Lesuffleur, A.; Kumar, L. K. S.; Brolo, A. G.; Kavanagh, K. L.; Gordon, R. Apex-Enhanced Raman Spectroscopy Using Double-Hole Arrays in a Gold Film. *J. Phys. Chem. C* **2007**, *111*, 2347–2350.

(15) Yu, Q.; Golden, G. Probing the Protein Orientation on Charged Self-Assembled Monolayers on Gold Nanohole Arrays by SERS. *Langmuir* **2007**, *23*, 8659–8662.

(16) Reilly, T. H.; Corbman, J. D.; Rowlen, K. L. Vapor Deposition Method for Sensitivity Studies on Engineered Surface-Enhanced Raman Scattering-Active Substrates. *Anal. Chem.* **2007**, *79*, 5078–5081.

(17) Yu, Q.; Guan, P.; Qin, D.; Golden, G.; Wallace, P. M. Inverted Size-Dependence of Surface-Enhanced Raman Scattering on Gold Nanohole and Nanodisk Arrays. *Nano Lett.* **2008**, *8*, 1923–1928.

(18) Anema, J. R.; Brolo, A. G.; Marthandam, P.; Gordon, R. Enhanced Raman Scattering from Nanoholes in a Copper Film. *J. Phys. Chem. C* **2008**, *112*, 17051–17055.

(19) Bahns, J. T.; Guo, Q.; Montgomery, J. M.; Gray, S. K.; Jaeger, H. M.; Chen, L. High-Fidelity Nano-Hole-Enhanced Raman Spectroscopy. *J. Phys. Chem. C* **2009**, *113*, 11190–11197.

(20) Wei, H.; Håkanson, U.; Yang, Z.; Höök, F.; Xu, H. Individual Nanometer Hole-Particle Pairs for Surface-Enhanced Raman Scattering. *Small* **2008**, *4*, 1296–1300.

(21) Min, Q.; Leite Santos, M. J.; Girotto, E. M.; Brolo, A. G.; Gordon, R. Localized Raman Enhancement from a Double-Hole Nanostructure in a Metal Film. *J. Phys. Chem. C* **2008**, *112*, 15098–15101.

(22) Mahdavi, F.; Liu, Y.; Blair, S. Modeling Fluorescence Enhancement from Metallic Nanocavities. *Plasmonics* **2007**, *2*, 129–142.

(23) Osawa, M.; Matsuda, N.; Yoshii, K.; Uchida, I. Charge transfer resonance Raman process in surface-enhanced Raman scattering from p-aminothiophenol adsorbed on silver: Herzberg-Teller contribution. *J. Phys. Chem.* **1994**, *98*, 12702–12707.

(24) Hill, W.; Wehling, B. Potential- and pH-dependent surface-enhanced Raman scattering of p-mercapto aniline on silver and gold substrates. *J. Phys. Chem.* **1993**, *97*, 9451–9455.

(25) Lombardi, J. R.; Birke, R. L. A Unified Approach to Surface-Enhanced Raman Spectroscopy. *J. Phys. Chem. C* **2008**, *112*, 5605–5617.

(26) Vanduyne, R. P.; Hulteen, J. C.; Treichel, D. A. Atomic-force microscopy and surface-enhanced Raman spectroscopy on Ag island films and Ag film over polymer nanosphere surfaces supported on glass. *J. Chem. Phys.* **1993**, *99*, 2101–2115.

(27) Le Ru, E. C.; Blackie, E.; Meyer, M.; Etchegoin, P. G. Surface Enhanced Raman Scattering Enhancement Factors: A Comprehensive Study. *J. Phys. Chem. C* **2007**, *111*, 13794–13803.

(28) Chang, S. H.; Gray, S. K.; Schatz, G. C. Surface plasmon generation and light transmission by isolated nanoholes and arrays of nanoholes in thin metal films. *Opt. Express* **2005**, *13*, 3150–3165.

(29) Gérard, D.; Wenger, J.; Bonod, N.; Popov, E.; Rigneault, H.; Mahdavi, F.; Blair, S.; Dintinger, J.; Ebbesen, T. W. Nanoaperture-Enhanced Fluorescence: Towards Higher Detection Rates with Plasmonic Metals. *Phys. Rev. B* **2008**, *77*, 045413.

(30) Wenger, J.; Gérard, D.; Dintinger, J.; Mahboub, O.; Bonod, N.; Popov, E.; Ebbesen, T. W.; Rigneault, H. Emission and Excitation Contributions to Enhanced Single Molecule Fluorescence by Gold Nanometric Apertures. *Opt. Express* **2008**, *16*, 3008–3020.

(31) Aouani, H.; Wenger, J.; Gérard, D.; Rigneault, H.; Devaux, E.; Ebbesen, T. W.; Mahdavi, F.; Xu, T.; Blair, S. Crucial Role of the Adhesion Layer on the Plasmonic Fluorescence Enhancement. *ACS Nano* **2009**, *3*, 2043–2048.

(32) Wenger, J.; Dintinger, J.; Bonod, N.; Popov, E.; Lenne, P.-F.; Ebbesen, T. W.; Rigneault, H. Raman scattering and fluorescence emission in a single nanoaperture: Optimizing the local intensity enhancement. *Opt. Commun.* **2006**, *267*, 224–228.

(33) Jiao, X.; Goeckeritz, J.; Blair, S.; Oldham, M. Localization of Near-Field Resonances in Bowtie Antennae: Influence of Adhesion Layers. *Plasmonics* **2009**, *4*, 37–50.

JP104971P